Published December 24, 2012

Plasma membrane calcium ATPase regulates bone mass by fine-tuning osteoclast differentiation and survival

Hyung Joon Kim,[1] Vikram Prasad,[2] Seok-Won Hyung,[3] Zang Hee Lee,[1] Sang-Won Lee,[3] Aditi Bhargava,[4] David Pearce,[5] Youngkyun Lee,[6] and Hong-Hee Kim[1]

[1]Department of Cell and Developmental Biology, BK21 Program and Dental Research Institute, Seoul National University, Seoul 110-749, Korea
[2]Department of Molecular Genetics, Biochemistry, and Microbiology, University of Cincinnati College of Medicine, Cincinnati, OH 45267
[3]Department of Chemistry, Korea University, Seoul 136-701, Korea
[4]Department of Surgery and [5]Department of Medicine, University of California, San Francisco, San Francisco, CA 94143
[6]Department of Biochemistry, School of Dentistry, Kyungpook National University, Daegu 700-412, Korea

The precise regulation of Ca^{2+} dynamics is crucial for proper differentiation and function of osteoclasts. Here we show the involvement of plasma membrane Ca^{2+} ATPase (PMCA) isoforms 1 and 4 in osteoclastogenesis. In immature/undifferentiated cells, PMCAs inhibited receptor activator of NF-κB ligand–induced Ca^{2+} oscillations and osteoclast differentiation in vitro. Interestingly, nuclear factor of activated T cell c1 (NFATc1) directly stimulated PMCA transcription, whereas the PMCA-mediated Ca^{2+} efflux prevented NFATc1 activation, forming a negative regulatory loop. PMCA4 also had an anti-osteoclastogenic effect by reducing NO, which facilitates preosteoclast fusion. In addition to their role in immature cells, increased expression of PMCAs in mature osteoclasts prevented osteoclast apoptosis both in vitro and in vivo. Mice heterozygous for PMCA1 or null for PMCA4 showed an osteopenic phenotype with more osteoclasts on bone surface. Furthermore, PMCA4 expression levels correlated with peak bone mass in premenopausal women. Thus, our results suggest that PMCAs play important roles for the regulation of bone homeostasis in both mice and humans by modulating Ca^{2+} signaling in osteoclasts.

Introduction

Bone homeostasis is maintained by the concerted action of bone-forming osteoblasts and bone-resorbing osteoclasts. In the bone microenvironment, osteoclast differentiation is governed by macrophage colony-stimulating factor (M-CSF) and receptor activator of nuclear factor κB ligand (RANKL) provided by osteoblasts, stromal cells, and lymphocytes (Boyle et al., 2003; Walsh et al., 2006). M-CSF ensures the survival of osteoclast precursors, and RANKL stimulates signaling pathways required for osteoclastogenesis (Boyle et al., 2003; Walsh et al., 2006). Upon maturation, osteoclasts tightly seal off bone surfaces and secrete acids and proteases to digest bone matrices.

The sophisticated control of both extracellular and intracellular Ca^{2+} concentrations is pivotal to the proper development and function of osteoclasts (Lorget et al., 2000; Nowycky and Thomas, 2002). During osteoclast differentiation by RANKL, cytosolic Ca^{2+} concentrations show an oscillatory pattern (Takayanagi et al., 2002; Asagiri et al., 2005). For the initiation of RANKL-dependent Ca^{2+} oscillation, the activation of PLCγ and the engagement of inositol 1,4,5-triphosphate receptor type2 have been suggested to be essential (Kuroda et al., 2008; Shinohara et al., 2008; Yoon et al., 2009). RANKL-induced Ca^{2+} oscillation triggers calcineurin-dependent dephosphorylation and nuclear translocation of nuclear factor of

Correspondence to Hong-Hee Kim: hhbkim@snu.ac.kr; or Youngkyun Lee: ylee@knu.ac.kr

Abbreviations used in this paper: BMM, bone marrow–derived macrophage; ChIP, chromatin immunoprecipitation; LC/MS/MS, liquid chromatography/mass spectrometry/mass spectrometry; M-CSF, macrophage colony-stimulating factor; μCT, microcomputed tomography; MEM, modified Eagle medium; NCX, Na^+/Ca^+ exchanger; NFATc1, nuclear factor of activated T cell c1; nNOS, neuronal NOS; NOS, nitric oxide synthase; PBMC, peripheral blood mononuclear cell; PMCA, plasma membrane Ca^{2+} ATPase; RANKL, receptor activator of NF-κB ligand; TRAP, tartrate-resistant acid phosphatase.

Supplemental Material can be found at:
http://jcb.rupress.org/content/suppl/2012/12/19/jcb.201204067.DC1.html

The Rockefeller University Press $30.00
J. Cell Biol. Vol. 199 No. 7 1145–1158
www.jcb.org/cgi/doi/10.1083/jcb.201204067

Published December 24, 2012

activated T cell c1 (NFATc1; Asagiri et al., 2005; Yang and Li, 2007). Because the activity of NFATc1 controls the transcription of osteoclastogenic genes (Asagiri et al., 2005; Walsh et al., 2006), the molecular mechanisms by which Ca^{2+} oscillations are generated and regulated are of great importance in the understanding of mechanisms for osteoclast differentiation. In addition, mature osteoclasts absorb vast amounts of Ca^{2+} accompanied by organic bone degradation products during resorption. Because excessive Ca^{2+} ions are toxic to osteoclasts, osteoclast survival is ensured by the extrusion of Ca^{2+} into the surrounding extracellular space via transcytosis (Salo et al., 1997) or certain Ca^{2+} transporters including Na^+/Ca^{2+} exchangers (Moonga et al., 2001; Li et al., 2007).

In proteomic and genomic screening experiments, we discovered that the expression of plasma membrane Ca^{2+} ATPase (PMCA) isoforms 1 and 4 was dramatically increased during the late phase of osteoclast differentiation. PMCA belongs to the P-type pump family that maintains intracellular Ca^{2+} homeostasis by exporting Ca^{2+} from the cytoplasm to the extracellular space (Di Leva et al., 2008; Brini, 2009). It was reported that PMCA1 knockout is lethal to mice during early embryonic development (Okunade et al., 2004). The major observed phenotype of PMCA4 knockout mice was male infertility as a result of reduced sperm motility (Schuh et al., 2004). Besides its role as a Ca^{2+} pump, PMCA has been suggested to function as a signaling molecule in recent studies (Buch et al., 2005; Cartwright et al., 2009). Of particular note, PMCA4 functionally interacts with nitric oxide synthase (NOS). Overexpression of PMCA4 dramatically down-regulated NO synthesis in the ambient Ca^{2+} concentration where NOS operates (Schuh et al., 2001).

Here, we report that PMCAs play dual roles in osteoclast differentiation and survival by regulating RANKL-induced Ca^{2+} oscillations in preosteoclasts and mediating Ca^{2+} extrusion in mature osteoclasts. Furthermore, PMCA deficiency induced a low bone mass phenotype in mice. In addition, high PMCA4 expression levels showed a positive correlation with peak bone mass in premenopausal women. These results suggest a novel role for PMCAs in osteoclast development and bone homeostasis.

Results

PMCAs are induced by RANKL during osteoclastogenesis

In an effort to identify new molecular players associated with osteoclastogenesis, we analyzed gene expression changes during osteoclast differentiation from human peripheral blood mononuclear cells (PBMCs) using DNA microarrays (Chang et al., 2008a). Among the genes significantly increased, *ATP2B4* (gene encoding PMCA4 Ca^{2+} pump) was present (Fig. 1 A). Interestingly, in a proteomic study involving cell-surface protein purification and subsequent liquid chromatography/mass spectrometry/mass spectrometry (LC/MS/MS) analyses, the protein level of PMCA1 was found to become higher in mouse osteoclast precursors upon stimulation with RANKL (Fig. 1 B; Lee et al., 2008). Among the four known isoforms of PMCA (Clapham, 2007; Brini, 2009), the mRNA levels of *Atp2b1* (gene encoding PMCA1) and *Atp2b4* prominently increased during osteoclastogenesis from mouse bone marrow–derived macrophages (BMMs), whereas *Atp2b2* (PMCA2) and *Atp2b3* (PMCA3) were not detected during the entire course of osteoclastogenesis (Fig. 1 C). In contrast, the expression of isoforms of Na^+/Ca^+ exchanger (NCX), a family of Ca^{2+} transporters expressed in mature osteoclasts (Moonga et al., 2002; Li et al., 2007), either decreased (*Slc8a1* [gene encoding NCX1]) or was undetectable during osteoclast differentiation (Fig. 1 D). Quantitative real-time PCR experiments (Fig. 1 E) and Western blot analyses using a pan-PMCA antibody (Fig. 1 F) further corroborated the up-regulation of PMCA at both the mRNA and protein levels during osteoclastogenesis from BMMs. Confocal microscopy studies revealed that PMCA localized to the basolateral membranes of mature osteoclasts cultured on dentin slices (Fig. 1 G). Although the question of whether PMCAs are also expressed on the apical (resorbing) membranes could not be clearly answered by confocal analyses of cells on dentin disc because of autofluorescence of dentin, exclusive basolateral localization of PMCA was evident in osteoclasts plated on glass coverslips (unpublished data).

The transcription factor NFATc1 is a key regulator of osteoclastogenesis and its expression is induced by RANKL (Takayanagi et al., 2002; Yang and Li, 2007). Notably, we found using the wed-based prediction program PROMO that the promoter regions of *Atp2b1* and *Atp2b4* contain several putative NFATc1 binding sites. To test the possibility of involvement of NFATc1 in the regulation of PMCA expression, we overexpressed a constitutive-active form of NFATc1 (NFATc1-CA) in BMMs. As shown in Fig. 1 H, NFATc1-CA overexpression was sufficient to induce PMCA expression in the absence of RANKL stimulation (Fig. 1 H). In addition, chromatin immunoprecipitation (ChIP) experiments revealed that NFATc1 bound to the promoter regions of *Atp2b1* and *Atp2b4* in RANKL-treated BMMs (Fig. 1 I). These data indicate that PMCA expression is up-regulated during osteoclastogenesis in an NFATc1-dependent manner and suggest the possibility that PMCAs extrude Ca^{2+} across the basolateral membrane of osteoclasts.

PMCA deficiency enhances osteoclastogenesis

Because the expression of PMCA isoforms significantly increased during osteoclastogenesis, their role for osteoclast differentiation was tested by introducing siRNA into mouse BMM osteoclast precursors. The isoform-specific knockdown of PMCA1 and PMCA4 was confirmed by RT-PCR analysis (Fig. 2 A) and Western blotting (Fig. 2 B). The PMCA siRNA-transfected BMMs were further cultured in the presence of RANKL to allow the formation of mature osteoclasts. The knockdown of PMCAs remarkably increased the formation of tartrate-resistant acid phosphatase (TRAP)–positive multinuclear osteoclasts compared with control siRNA-transfected cells (Fig. 2 C, top). The increased osteoclastogenesis by PMCA knockdown resulted in a significantly enhanced resorption (Fig. 2 C, bottom), indicating the osteoclasts generated were functionally competent.

Published December 24, 2012

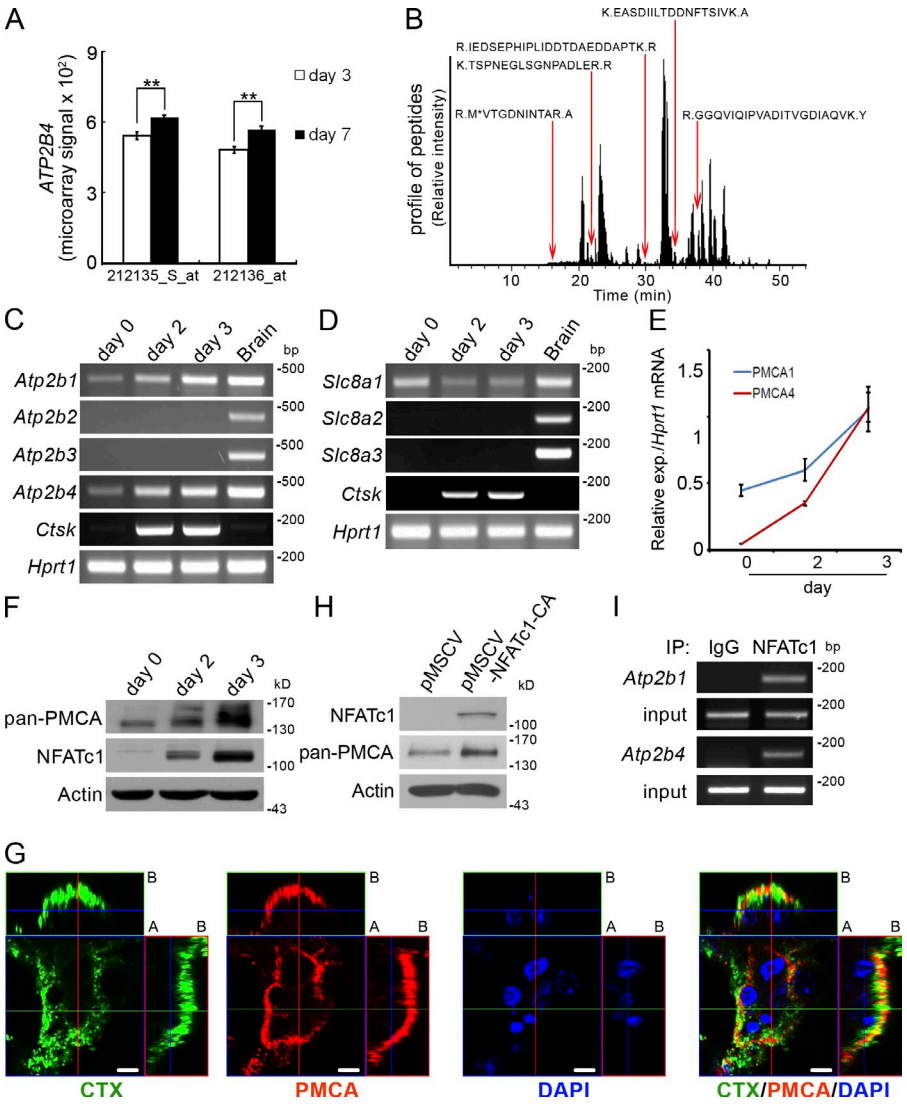

Figure 1. **PMCA expression was increased during RANKL-induced osteoclast differentiation.** (A) Human PBMCs were cultured in the presence of 30 ng/ml M-CSF and 100 ng/ml RANKL. After 3 and 7 d of culture (preosteoclast and mature osteoclast stages, respectively), total RNAs were extracted and subjected to DNA microarray analysis. The relative signal intensity of *ATP2B4* (the gene encoding PMCA4) mRNA detected in a DNA microarray analysis is shown. Data are means ± SD (**, $P < 0.01$). (B) Mouse BMMs were incubated with 30 ng/ml M-CSF or M-CSF plus 100 ng/ml RANKL for 36 h. Biotinylated cell surface proteins were prepared as described in Materials and methods and subjected to LC/MS/MS analysis. The elution profile of peptides from LC is shown. Arrows indicate PMCA1 peptides identified by subsequent mass spectrometry analyses. (C and D) Mouse BMMs were stimulated with 100 ng/ml RANKL in the presence of 30 ng/ml M-CSF for the indicated times. Total RNA was subjected to RT-PCR analysis to examine the expression levels of *Atp2b* and *Slc8a* families (the genes encoding NCXs). The mRNA expression in mouse brain was used as a positive control. *Ctsk* (cathepsin K) is a marker gene for osteoclast differentiation. (E) Quantitative real-time PCR analysis of *Atp2b1* and *Atp2b4* transcripts was performed with BMMs treated with 100 ng/ml RANKL plus 30 ng/ml M-CSF for the indicated times. The mRNA expression levels were normalized against those of *Hprt1*. The error bars show the mean ± SD of three independent experiments. (F) Cell lysates from BMMs treated with 100 ng/ml RANKL plus 30 ng/ml M-CSF for the indicated times were subjected to Western blotting. The expression levels of total PMCA and NFATc1 were examined with pan-PMCA and NFATc1 antibodies. (G) PMCA immunostaining (Cy3) was performed with mature mouse osteoclasts cultured on dentin discs. Plasma membrane ganglioside GM1 was co-stained using FITC-conjugated cholera toxin B. Cross-sectional images were reconstructed through the z-axis by confocal microscopy (A, apical; B, basolateral). Bars, 5 µm. (H) BMMs were infected with viruses harboring empty vector (pMSCV) or constitutively active NFATc1 (pMSCV-NFATc1-CA). 2 d after infection, PMCA and NFATc1 expression was examined by Western blotting. (I) BMMs were treated with 100 ng/ml RANKL plus 30 ng/ml M-CSF for 2 d. ChIP was performed using an NFATc1 antobody followed by a PCR amplification of the promoter regions of *Atp2b1* or *Atp2b4* gene. Input DNA (1% of total) was also amplified using the same primer sets.

Because PMCA knockdown increased osteoclast number and size (Fig. 2 C, top), the expression of osteoclast marker genes was analyzed by quantitative real-time PCR (Fig. 2 D). The knockdown of PMCA1 and PMCA4 significantly augmented the induction of fusion marker genes *Tm7sf4* (DC-STAMP) and *Atp6v0d2* (V-ATPase) as well as differentiation marker genes *Ctsk* (cathepsin K) and *Acp5* (TRAP) by RANKL stimulation. BMMs obtained from *Atp2b1*$^{+/-}$ (PMCA1-heterozygous) and *Atp2b4*$^{-/-}$(PMCA4-null) mice also exhibited significantly accelerated osteoclastogenesis in vitro, compared with wild-type cells (Fig. 2 E). Finally, the in vivo effect of PMCA knockdown was analyzed after injecting PMCA-targeting siRNA oligonucleotides onto mouse calvariae. A microcomputed tomography (µCT) analysis (Fig. 2 F, top) and TRAP staining (Fig. 2 F, bottom) of calvarial bones clearly revealed that bone resorption as well as osteoclast formation increased significantly in the absence of PMCA, with concomitant up-regulation of the TRAP gene expression (Fig. 2 G). Similarly, enhanced osteoclastogenesis was observed when PMCA was silenced in calvariae organ culture experiments (Fig. S1).

PMCAs regulate the Ca^{2+} oscillation–NFATc1 axis in preosteoclasts

It has been suggested that RANKL-induced Ca^{2+} oscillations are crucial for the maintenance of cytosolic Ca^{2+} concentration required for osteoclast differentiation (Takayanagi et al., 2002; Walsh et al., 2006; Shinohara et al., 2008). Eosin (tetrabromofluorescein) has been suggested as a potent inhibitor of PMCAs (IC_{50} = 1 µM; Gatto and Milanick, 1993; Gatto et al., 1995). Treatment of eosin not only strongly enhanced RANKL-induced Ca^{2+} oscillations in preosteoclasts in vitro but also augmented the formation of osteoclasts in vivo (Fig. S2). Consistently, the knockdown of PMCA1 or PMCA4 induced robust Ca^{2+} oscillations in preosteoclasts (Fig. 3 A). NFATc1 is a

Published December 24, 2012

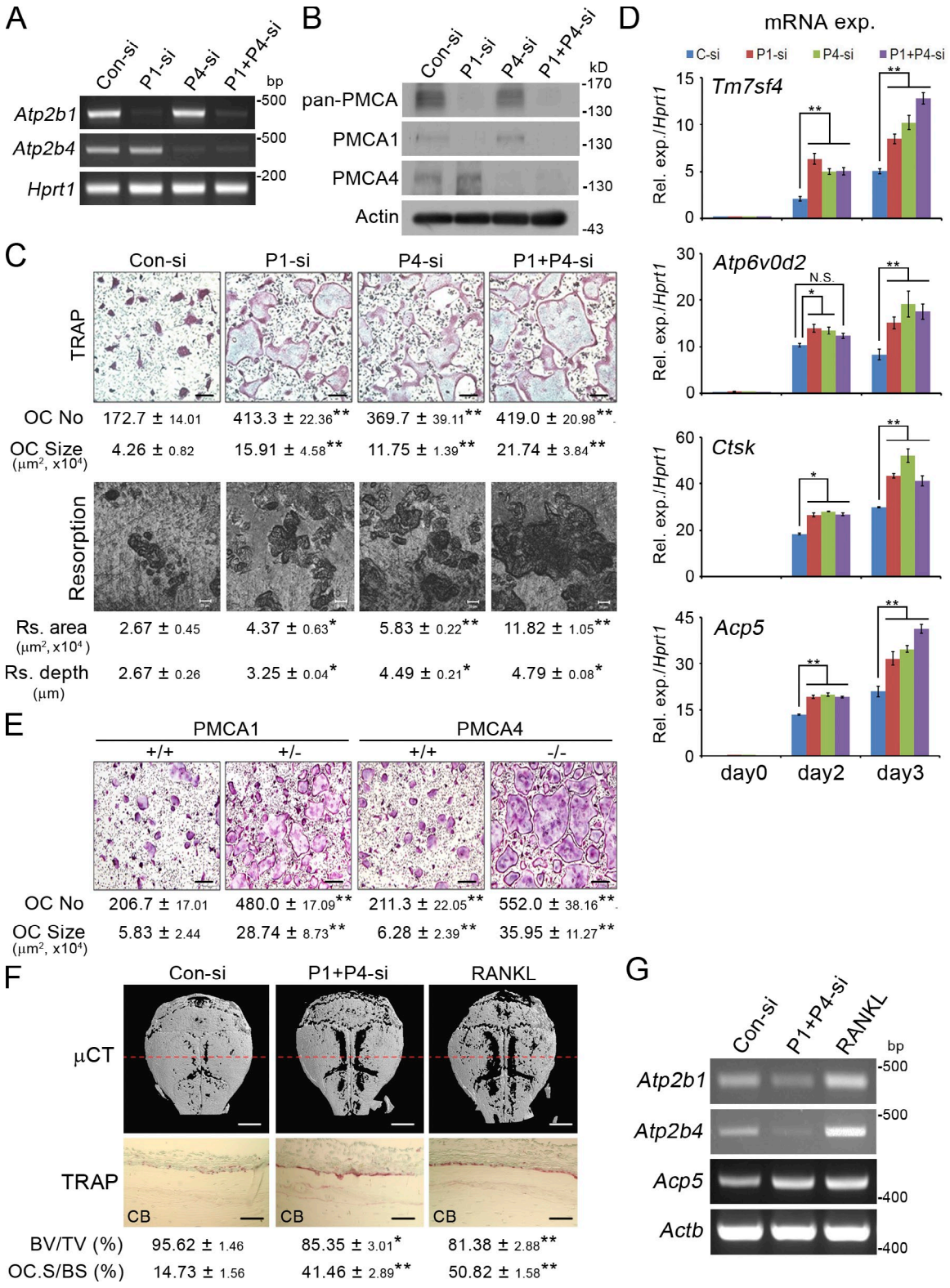

Figure 2. **PMCA deficiency enhanced osteoclast differentiation.** (A–D) BMMs were transfected with scrambled control siRNA oligonucleotides (Con-si) or isoform-specific PMCA1 (P1-si) or PMCA4 (P4-si) siRNA and further cultured in the presence of 100 ng/ml RANKL and 30 ng/ml M-CSF. At 48 h after transfection, PMCA mRNA (A) and protein (B) levels were examined. (C) TRAP staining was performed after culturing BMMs with 100 ng/ml RANKL and 30 ng/ml M-CSF for 3 d (top). Bars, 200 µm. For the examination of resorption activities, BMMs plated on dentin discs were cultured in the presence of RANKL plus M-CSF for 5 d. Resorption pits were visualized by a confocal laser scanning of dentin discs (bottom). Bars, 50 µm. OC, osteoclast. (D) The mRNA expression of *Tm7sf4* (DC-STAMP), *Atp6v0d2* (V-ATPase), *Ctsk* (cathepsin K), and *Acp5* (TRAP) was analyzed by quantitative real-time PCR after culturing BMMs in the presence of 100 ng/ml RANKL and 30 ng/ml M-CSF for the indicated times. (E) *Atp2b1*$^{+/-}$, *Atp2b4*$^{-/-}$, and corresponding wild-type BMMs were stimulated with 100 ng/ml RANKL plus 30 ng/ml M-CSF for 3 d and stained for TRAP activity. Bars, 200 µm. (F and G) The in vivo knockdown of PMCA was performed by injecting siRNA oligonucleotides into the subcutaneous space on mouse calvariae. (F) A 3D reconstruction of µCT images of

Published December 24, 2012

Ca^{2+}-dependent key transcription factor for osteoclastogenesis (Kim et al., 2005; Sharma et al., 2007). The dephosphorylation of NFATc1 by calcineurin followed by nuclear translocation and binding to its own promoter up-regulates NFATc1 expression during osteoclast differentiation through a process called auto-amplification (Asagiri et al., 2005). In accordance with the increased Ca^{2+} oscillations, both PMCA1 and PMCA4 siRNA significantly increased the number of cells with nuclear NFATc1, whereas the addition of a calcineurin inhibitor cyclosporine A almost completely abolished NFATc1 nuclear localization (Fig. 3, B and C). Western blotting analyses further confirmed elevated NFATc1 levels in nuclear fractions of PMCA knockdown cells (Fig. 3 D). In sharp contrast to the PMCA knockdown, the overexpression of rat PMCA1 or mouse PMCA4 in BMMs (Fig. 3 F) strongly suppressed RANKL-dependent Ca^{2+} oscillations (Fig. 3 E) as well as osteoclastogenesis (Fig. 3, E and G). However, the silencing of PMCA1 and PMCA4 did not markedly alter other receptor activators of NF-κB signaling pathways including the phosphorylation of MAPKs, the expression of c-Jun and c-Fos, or the activation of PLCγ1 (Fig. S3).

PMCAs regulate bone homeostasis in vivo

To examine the in vivo role of PMCAs in bone homeostasis, femurs from *Atp2b1*$^{+/-}$ (PMCA1-heterozygous) and *Atp2b4*$^{-/-}$ (PMCA4-null) mice were analyzed. The von Kossa staining of femurs from 6-wk-old male mice revealed a lower amount of mineralized bone in both *Atp2b1*$^{+/-}$ and *Atp2b4*$^{-/-}$ mice compared with respective wild-type mice (Fig. 4 A). Similarly, the μCT analyses of metaphyseal regions of femurs showed lower trabecular bone volume and bone mineral density in both PMCA-insufficient mice (Fig. 4 A). Finally, histological assessments confirmed a significant reduction in trabecular bone volumes (hematoxylin and eosin staining) and a marked increase in the osteoclast surface (TRAP staining) in *Atp2b1*$^{+/-}$ and *Atp2b4*$^{-/-}$ mice compared with wild-type mice. These effects of PMCA deficiency on bone homeostasis were osteoclast specific because the number of osteoblasts was similar in both PMCA-insufficient mice to that of corresponding wild-type mice (Fig. 4 A). Furthermore, the mineral apposition rate was not significantly different in *Atp2b1*$^{+/-}$ or *Atp2b4*$^{-/-}$ mice compared with wild-type mice (Fig. 4 B). In addition, the knockdown of PMCA expression or the inhibition of PMCA activity in calvarial cells did not affect osteoblast differentiation in vitro (Fig. S4).

PMCAs facilitate the survival of bone-resorbing mature osteoclasts

Intracellular Ca^{2+} overload is highly toxic to cells. The disposal of surplus intracellular Ca^{2+} is particularly important in mature osteoclasts because massive Ca^{2+} influx occurs when osteoclasts resorb the mineral components of bone (Salo et al., 1997). In this context, we hypothesized that increased PMCA expression in mature osteoclasts might facilitate the removal of intracellular Ca^{2+} during bone resorption, preventing Ca^{2+}-induced apoptosis. To test this hypothesis, the TUNEL staining was performed with trabecular bone sections of femurs from *Atp2b1*$^{+/-}$ and *Atp2b4*$^{-/-}$ mice. Both PMCA-deficient mice exhibited conspicuously more TUNEL-positive osteoclasts compared with wild-type mice (Fig. 5, A and B), supporting the notion of an anti-apoptotic role for PMCAs in mature osteoclasts. When cultured on dentin slices in vitro, osteoclasts derived from *Atp2b1*$^{+/-}$ and *Atp2b4*$^{-/-}$ mice also showed more apoptotic nuclei compared with wild-type cells (Fig. 5, C and D). To further examine the role of PMCAs in bone-resorbing osteoclasts, isolated mature osteoclasts were transfected with PMCA siRNAs and cultured on dentin slices. The TUNEL staining of these osteoclasts showed a significantly higher number of TUNEL-positive cells in PMCA-silenced culture (Fig. 5, E and F). In addition, PMCA-silencing in osteoclasts promoted the cleavage of PARP and caspase-3 upon ionomycin treatment (Fig. 5 G), indicating that osteoclasts are more susceptible to Ca^{2+}-induced apoptosis in the absence of PMCAs. The increase in apoptosis led to a marked reduction in resorbed areas on dentin slices when PMCAs were silenced in mature osteoclasts, although slightly deeper resorption pits were formed upon the knockdown of PMCAs (Fig. 5 H). Similar enhancement of apoptosis by PMCA siRNA was also observed when osteoclasts were grown on glass slides and challenged with ionomycin to mimic Ca^{2+} entry during bone resorption, whereas the overexpression of PMCAs strongly prevented Ca^{2+}-induced apoptosis (Fig. 5, I and J).

PMCA4 but not PMCA1 is involved in NO-dependent osteoclast fusion

The knockdown of PMCA4 alone induced comparable acceleration of osteoclast differentiation, despite that the PMCA1 isoform was dominantly expressed over PMCA4 in osteoclast precursors (Figs. 1 and 2). This result may suggest a possibility of additional function of PMCA4 involved in the regulation of osteoclastogenesis. Interestingly, PMCA4 was suggested to inhibit NO production (Schuh et al., 2001), which is known to promote the fusion of preosteoclasts in the late phase of osteoclastogenesis (Nilforoushan et al., 2009). As shown in Fig. 6 A, the Ca^{2+}-dependent neuronal NOS (nNOS) expression was significantly increased upon RANKL stimulation of BMMs. Furthermore, PMCA4 physically interacted with nNOS in preosteoclasts, whereas PMCA1 did not (Fig. 6 B). The knockdown of PMCA4, but not that of PMCA1, significantly enhanced NO production in preosteoclasts (Fig. 6 C). NOC-12, an NO donor, greatly augmented the size of osteoclasts, supporting the role of NO in preosteoclast fusion (Fig. 6 D). Although both PMCA1 and PMCA4 siRNA increased the formation of larger osteoclasts, only the PMCA4 siRNA-induced development of large osteoclasts was

calvariae is shown (top). Bars, 1 mm. Decalcified calvariae tissue sections along the dotted red line were stained for TRAP activity and counterstained with toluidine blue (bottom). Bars, 100 μm. The bone volume/tissue volume (BV/TV) and osteoclast surface/bone surface (OC.S/BS) were calculated from μCT and histomorphometry, respectively. CB denotes calvarial bones. (G) The mRNA levels of *Atp2b1*, *Atp2b4*, and *Acp5* in calvariae were examined by RT-PCR. All quantitative data are means ± SD ($n = 5$; *, $P < 0.05$; **, $P < 0.01$).

Published December 24, 2012

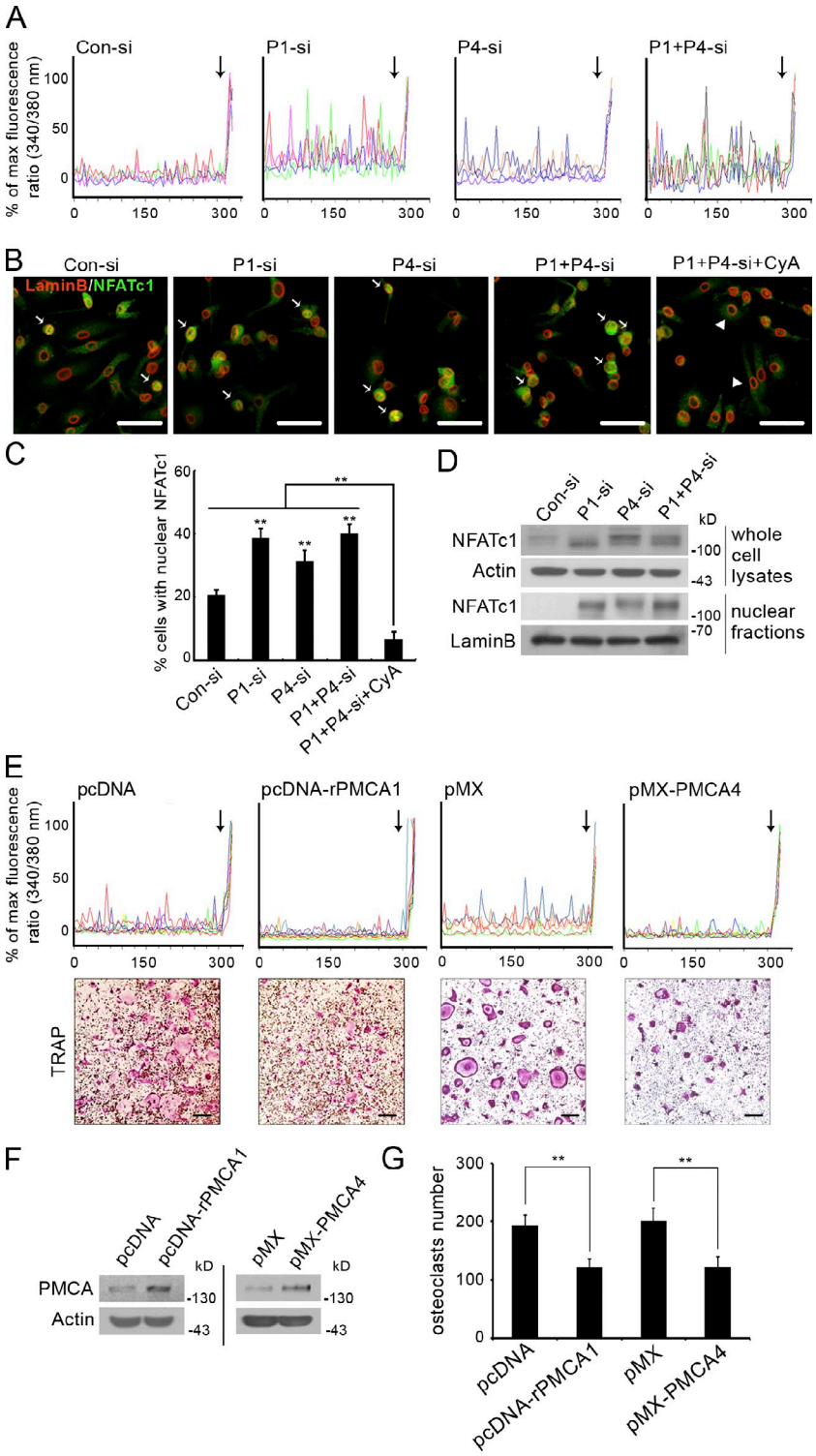

Figure 3. **PMCA reduced the RANKL-dependent Ca^{2+} oscillations and subsequent NFATc1 nuclear localization in preosteoclasts.** (A–C) BMMs on glass coverslips were transfected with scrambled control siRNA or PMCA siRNA and further incubated for 2 d with 30 ng/ml M-CSF and 100 ng/ml RANKL. (A) Cells were loaded with Fura-2/AM for the recording of Ca^{2+} oscillations (presented as a ratio of maximal fluorescence) in individual preosteoclast (BMMs treated with RANKL for 2 d). Each colored line represents Ca^{2+} oscillations in a single cell. 10 µM ionomycin was added at the end of the experiment (arrow) to determine the maximal Ca^{2+}-induced fluorescence. (B and C) Cells were stained with NFATc1 antibody (FITC labeled) and lamin B antibody (Cy3 labeled) to detect the nuclear localization of NFATc1 (arrows). Treatment of 1 µM cyclosporineA (CyA) for 3 h induced exclusive translocation of NFATc1 to the cytosol (arrowheads). Bars, 50 µm. (D) NFATc1 localization was examined biochemically by subjecting nuclear fractions from the cells treated as in B to Western blotting. (E and F) PMCA1 (pcDNA-rPMCA1) or PMCA4 (pMX-PMCA4) were overexpressed in BMMs. (E) Ca^{2+} oscillations were monitored in BMMs after RANKL treatment for 2 d (top). TRAP staining was performed after culturing the cells for 4 d (bottom). Bars, 200 µm. (F) PMCA1 or PMCA4 expression levels were examined by Western blotting after culturing the cells for 2 d. (G) The number of TRAP-positive multinucleated cells was counted from E. Data are means ± SD, representative of more than three experiments performed in triplicate (**, $P < 0.01$).

inhibited by the NOS inhibitor L-NMMA (Fig. 6, D and E). To further delineate the role of PMCA4 in nNOS-mediated osteoclasts fusion, siRNA oligonucleotides targeting nNOS were introduced into PMCA-silenced preosteoclasts, which were further cultured in the presence of RANKL to allow the formation of mature osteoclasts with the confirmation of specific knockdown by Western blotting (Fig. 6, F and G). The knockdown of nNOS only slightly reduced the osteoclast fusion index (Kaneda et al., 2000) in control and PMCA1-silenced cells (Fig. 6 H). However, nNOS siRNA dramatically reduced the osteoclasts fusion index in PMCA4-silenced osteoclast precursors. These data support the role of PMCA4 in regulating NO production and osteoclast fusion by inhibiting nNOS activity.

High PMCA4 gene expression correlates with high peak bone mass in humans

With ample evidence for PMCA in osteoclast regulation in mice, we next sought to investigate the potential association between

Published December 24, 2012

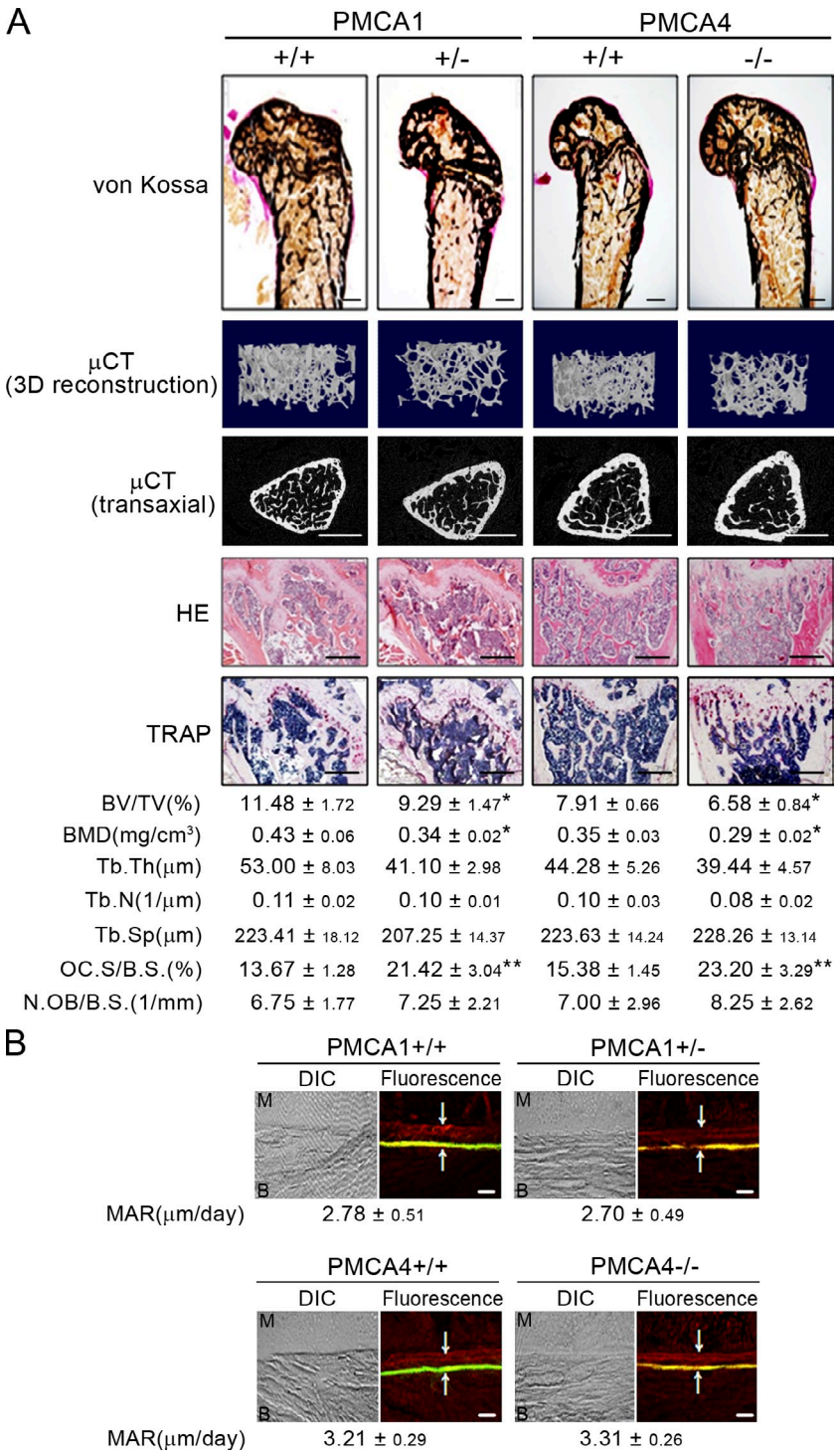

Figure 4. **PMCA-deficient mice show an osteopenic bone phenotype.** (A) Sections of femurs embedded in methyl methacrylate from 6-wk-old male *Atp2b1*$^{+/-}$, *Atp2b4*$^{-/-}$, and corresponding wild-type littermate mice were subjected to von Kossa/van Geison staining (top). Bars, 500 µm. After µCT analyses, 3D reconstruction and transaxial images were shown (middle). Bars, 1 mm. The hematoxylin/eosin (HE) and TRAP staining were performed with tibiae sections embedded in paraffin (bottom). Bars, 200 µm. (B) The mineral apposition rate was measured in endocortical bones of tibia sections embedded in methyl methacrylate after intraperitoneal injection of calcein (green) followed by xylenol orange (red). The fluorescence-labeled margins of cortical bones are indicated by arrows. Bars, 50 µm. B, bone; M, marrow space. Data are means ± SD (n = 5; **, P < 0.01; *, P < 0.05).

PMCA gene expression and bone homeostasis in humans. To this end, we analyzed a set of publicly available genomics data deposited in GEO (accession no. GSE7158) in which DNA microarray experiments were performed using blood monocytes obtained from 878 healthy Chinese women aged between 20 and 45. The microarray results were compared between 12 subjects with lowest peak bone mass and 14 subjects with highest peak bone mass. In this dataset, PMCA4 gene (*ATP2B4*) expression exhibited a significantly higher level in women with high peak bone mass (Fig. 7, A and B).

Discussion

The precise regulation of Ca^{2+} dynamics is crucial for proper differentiation and function of osteoclasts. RANKL induces oscillations of intracellular Ca^{2+} concentrations that trigger NFATc1 activation, which is a prerequisite for osteoclast differentiation. For the initiation of RANKL-dependent Ca^{2+} oscillations in osteoclasts, PLCγ activation is essential (Shinohara et al., 2008; Yoon et al., 2009). Furthermore, Kuroda et al., (2008) reported that the inositol 1,4,5-triphosphate receptor was

Published December 24, 2012

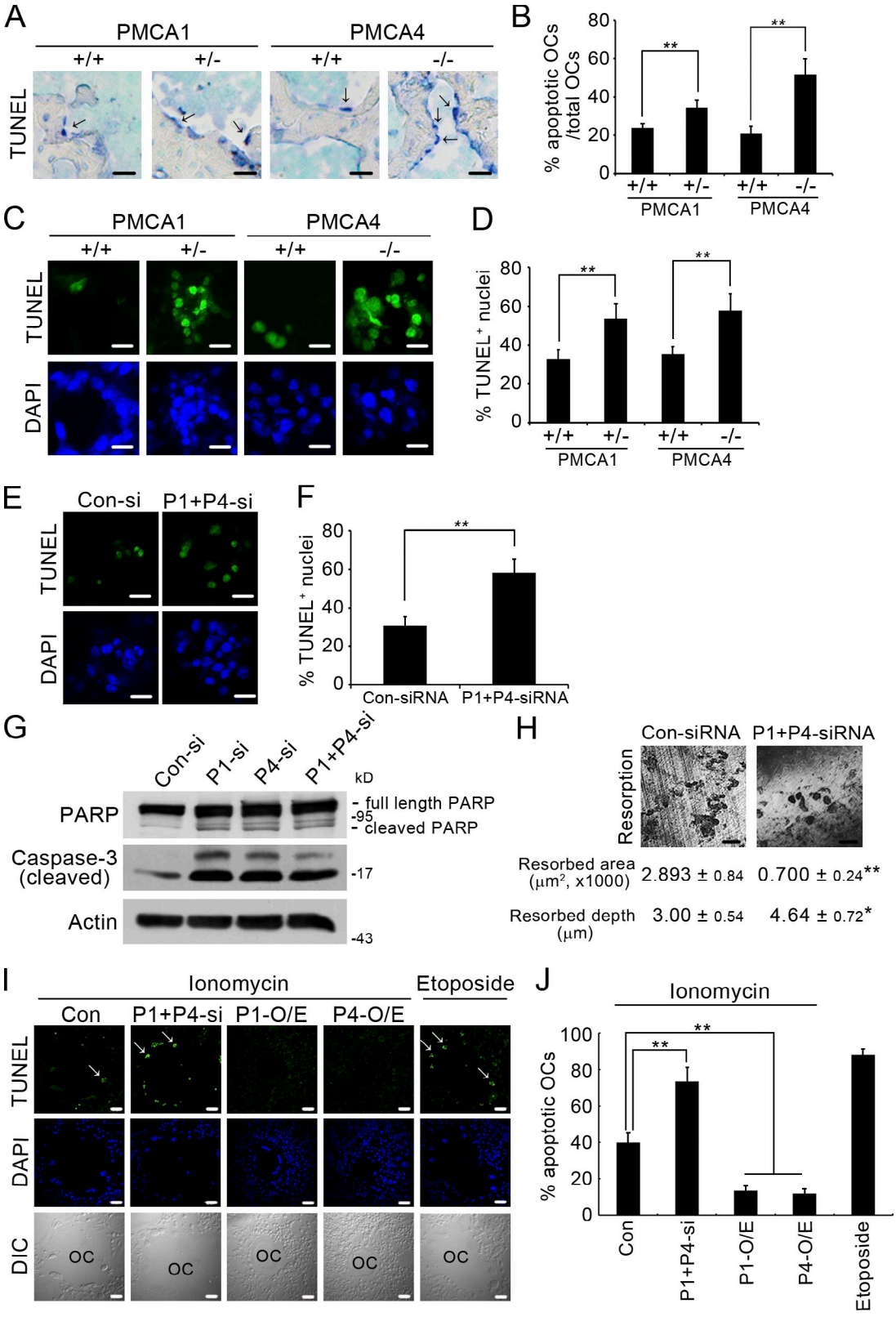

Figure 5. **PMCA enhanced the survival of mature osteoclasts.** (A and B) In situ TUNEL assay was performed in sections of tibiae embedded in paraffin from 6-wk-old male *Atp2b1*$^{+/-}$, *Atp2b4*$^{-/-}$, and corresponding wild-type littermate mice. (A) Arrows indicate apoptotic osteoclasts on bone surfaces. Bars, 100 µm. (B) The number of TUNEL-positive osteoclasts per total number of osteoclasts was quantified. Data are means ± SD of the representative experiment performed in quintuplicate ($n = 5$; **, $P < 0.01$). (C and D) Mature osteoclasts derived from *Atp2b1*$^{+/-}$, *Atp2b4*$^{-/-}$, and corresponding wild-type BMMs were plated on dentin discs. (C) After 2 d of mature osteoclasts culture, apoptotic osteoclasts on dentin discs were evaluated by TUNEL staining (green). Nuclei were shown by DAPI staining. Bars, 20 µm. (D) The number of TUNEL-positive nuclei per total number of nuclei was counted. (E and F) Mature osteoclasts on dentin discs were transfected with control siRNA (Con-si) or siRNAs against PMCA1 and PMCA4 (P1+P4-si). (E) After 2 d, apoptotic osteoclasts

Published December 24, 2012

critical for RANKL-induced Ca^{2+} oscillations and osteoclastogenesis. However, mechanisms for the termination of Ca^{2+} oscillations remain unknown although Ca^{2+} oscillations gradually disappear in the late stages of osteoclastogenesis. In the present study, we showed that the expression of two major Ca^{2+} extrusion pumps, PMCA1 and PMCA4, increased dramatically during the late stages of osteoclast differentiation (Fig. 1). Notably, overexpression of PMCAs in osteoclast precursors dramatically diminished the amplitudes of Ca^{2+} oscillations, reducing the osteoclastogenic potential (Fig. 3). In contrast, the knockdown of PMCAs resulted in a marked increase in Ca^{2+} oscillations. Consistent with these in vitro data, radiological and histomorphometric analyses of *Atp2b1*$^{+/-}$ and *Atp2b4*$^{-/-}$ mice revealed increased osteoclastogenesis with concomitant reduction of bone volume without any difference in bone formation (Fig. 4). To our knowledge, this study is the first demonstration that the plasma membrane Ca^{2+} pump is directly involved in the regulation of RANKL-induced Ca^{2+} oscillations and osteoclast differentiation both in vitro and in vivo. Interestingly, the knockdown of both PMCA1 and PMCA4 isoforms slightly increased the expression SERCA2 and reduced that of TRPV5 (Fig. S5), both of which have been shown to regulate cytosolic Ca^{2+} concentrations in osteoclasts (van der Eerden et al., 2005; Yang et al., 2009). However, it is highly unlikely that the observed pro-osteoclastogenic effects induced by PMCA deficiency were mainly caused by the indirect regulation of those proteins because individual knockdown of PMCA1 or PMCA4 significantly increased Ca^{2+} oscillations and osteoclastogenesis without conspicuous alterations in the SERCA2 and TRPV5 expression. Nonetheless, detailed dissection on the cross talk between the Ca^{2+} regulators in osteoclasts such as PMCA, SERCA, and TRPV is required to fully understand the mechanism by which osteoclast Ca^{2+} oscillations are controlled.

The transcriptional induction of PMCA genes was dependent on NFATc1 activity (Fig. 1). The promoter region of *Atp2b1* and *Atp2b4* contained several putative NFATc1 binding sites that indeed associated with NFATc1 (Fig. 1 I). Combined with the observation that the NFATc1 nuclear translocation was significantly increased in PMCA-silenced cells (Fig. 3 B), it is likely that an NFATc1-PMCA negative regulatory loop is operating to fine-tune osteoclast differentiation. We have reported such feedback regulation of NFATc1 by dual specificity tyrosine kinase 1A and Nogo-A during osteoclastogenesis (Lee et al., 2009, 2012). Thus, these data add another line of evidence that NFATc1 activity is regulated by positive and negative feedback mechanisms.

In our experiments, the increased expression of PMCAs persisted during osteoclastogenesis and reached a maximal level in mature osteoclasts (Fig. 1), leading to the hypothesis that these Ca^{2+} pumps might have additional roles in mature osteoclasts in addition to their role to diminish Ca^{2+} oscillations in developing osteoclasts. During bone resorption, a large amount of Ca^{2+} released from the bone enters osteoclasts via several Ca^{2+} transporters or channels localized on the apical membrane of osteoclasts including a plasma membrane ryanodine receptor (Moonga et al., 2002), TRPV5 (van der Eerden et al., 2005), and NCX (Li et al., 2007). Because high intracellular Ca^{2+} can be toxic to osteoclasts, excessive Ca^{2+} needs to be sequestered from the cytosol or expelled into the extracellular space. In this context, a continuous discharge of Ca^{2+} across the basolateral membrane has been observed in bone-resorbing osteoclasts (Berger et al., 2001). Although a Ca^{2+}-ATPase activity was discovered in the purified plasma membranes in chicken osteoclasts over two decades ago (Bekker and Gay, 1990), studies on its identification and function in osteoclasts have not been thoroughly performed until the present. Here we suggest that PMCAs localized on the basolateral membrane of mature osteoclasts (Fig. 1) might operate to extrude superfluous intracellular Ca^{2+} across the basolateral membrane to prevent Ca^{2+}-induced apoptosis of osteoclasts. In support of this hypothesis, we observed a significantly higher number of apoptotic osteoclasts in *Atp2b1*$^{+/-}$ mice and *Atp2b4*$^{-/-}$ mice compared with that of wild-type mice (Fig. 5). These results were further supported by in vitro experiments in which the knockdown of PMCAs resulted in a dramatically enhanced apoptosis in osteoclasts either cultured on bone slices or on glasses (Fig. 5, E and I). It should be noted that the plasma membrane NCX is another candidate considered for the removal of intracellular Ca^{2+} from osteoclasts. However, we observed that the mRNA expression of *Ncx1* (*Slc8a1*) dramatically decreased during osteoclast differentiation, whereas the transcripts of *Ncx2* and *Ncx3* were not detected during osteoclastogenesis (Fig. 1 D). Furthermore, a recent publication by Li et al., (2007) predicted that NCX works in an influx mode on apical membranes promoting the entry of Ca^{2+} present in resorption lacunae into bone-resorbing osteoclasts. Combined with the reported anti-apoptotic roles of PMCA in HepG2, HeLa, mouse smooth muscle cells, and T cells (Chami et al., 2003; Okunade et al., 2004; Pellegrini and Scorrano, 2007), the up-regulation of PMCA expression in bone-resorbing osteoclasts might be beneficial in preventing apoptosis by extruding excessive Ca^{2+}.

on dentin discs were assessed by TUNEL assay (green). Nuclei were visualized by DAPI staining. Bars, 20 µm. (F) The number of TUNEL-positive nuclei was quantified. The error bars show the mean ± SD of the representative experiment performed in quintuplicate (**, $P < 0.01$). (G) Mature osteoclasts were transfected with control (Con-si) or isoform-specific siRNAs targeting PMCA1 (P1-si) or PMCA4 (P4-si). After 24-h incubation, cells were treated with 10 µM ionomycin for 16 h. PARP/caspases-3 cleavage was examined by Western blotting. (H) Dentin discs used in E were observed under confocal laser scanning microscope after lysing cells with 0.5% Triton X-100. Both resorbed area and resorption depth were quantified using LSM image browser 4.2 (Carl Zeiss). Data are means ± SD from the representative of three experiments performed in seven replicates (**, $P < 0.01$; *, $P < 0.05$). Bar, 50 µm. (I) PMCAs were either knocked down or overexpressed by transfecting BMMs with siRNA oligonucleotides (P1+P4-si) or PMCA overexpression constructs (P1-O/E and P4-O/E). After differentiation into mature osteoclasts by RANKL treatment for 4 d, cells were treated with 1 µM ionomycin for 16 h before DAPI and TUNEL (green) staining followed by observation under a confocal microscope. As a positive control for apoptosis, etoposide treatment (50 µM, 16 h) was included. The TUNEL-positive apoptotic nuclei are indicated by arrows. Bars, 50 µm. (J) The percentage of osteoclasts containing more than three TUNEL-positive nuclei was calculated. Data are means ± SD, representative of three experiments performed in triplicate (**, $P < 0.01$).

Published December 24, 2012

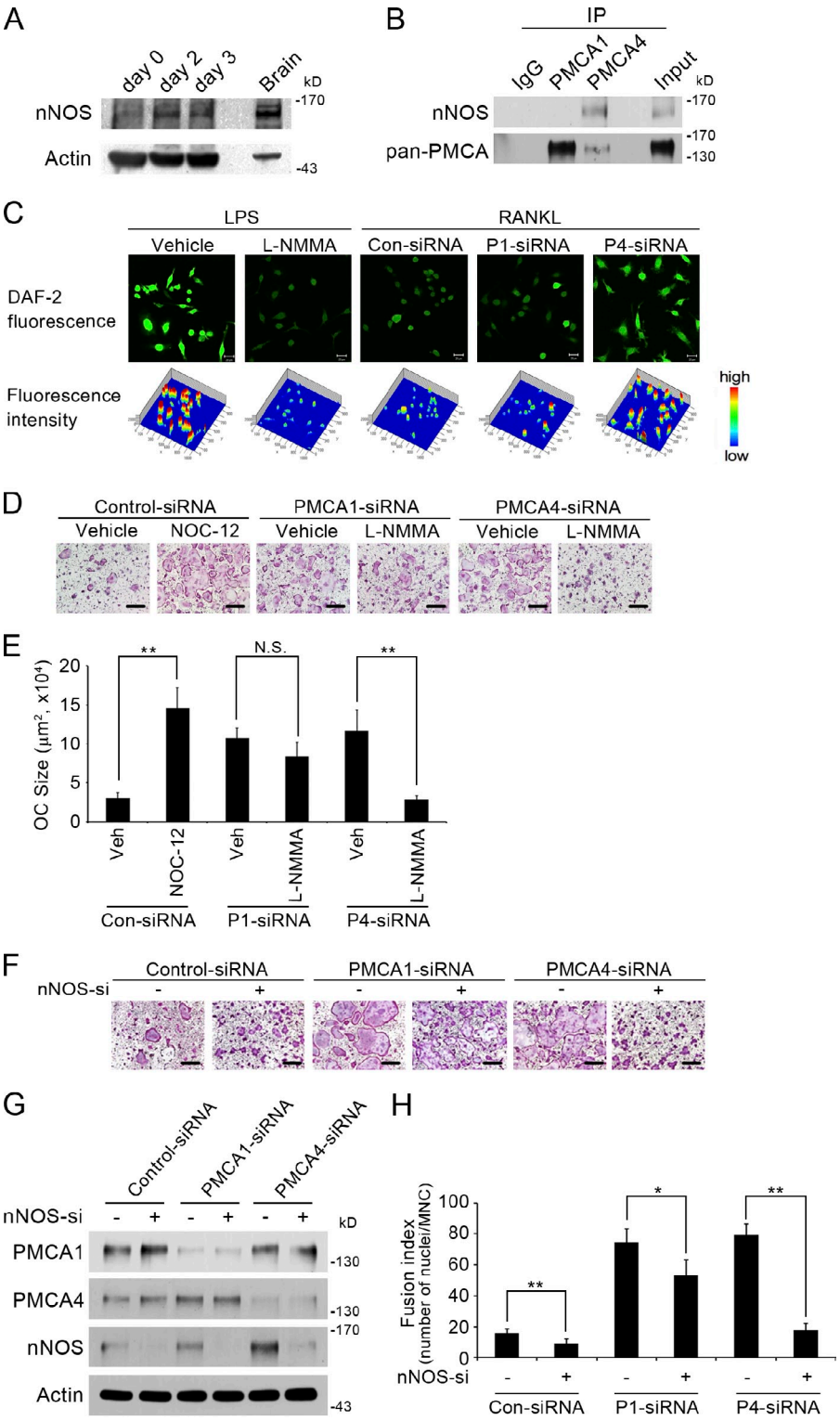

Figure 6. **PMCA4 but not PMCA1 inhibits NO generation in osteoclast precursors.** (A) BMMs were cultured in the presence of 100 ng/ml RANKL and 30 ng/ml M-CSF for the indicated times. Cell lysates were subjected to Western blotting to examine the expression levels of nNOS protein. The mouse brain lysates were used as positive control. (B) BMMs were incubated for 2 d with 30 ng/ml M-CSF and 100 ng/ml RANKL. After cell lysis, immunoprecipitation was performed with an antibody against PMCA1 or PMCA4. Immunoprecipitated proteins were detected by anti-nNOS or anti-pan-PMCA antibodies. (C) BMMs on glass coverslips were transfected with control siRNA or isoform-specific PMCA siRNA and further incubated with RANKL and M-CSF for 2 d. Cells were loaded with an NO indicator dye, DAF-2 DA. As a positive control, cells were stimulated overnight with 100 ng/ml LPS. As a negative control, cells were pretreated with NO synthase inhibitor L-NMMA (10 μM) for 2 h, and further cultured overnight with 100 ng/ml LPS. Bars, 20 μm. (D and E) BMMs were transfected with control siRNA or isoform-specific PMCA siRNA and cultured in the presence of RANKL and M-CSF for 4 d. The NO donor NOC-12 or L-NMMA was included for the final 2 d. (D) Cells were stained for TRAP activity. Bars, 200 μm. (E) The size of osteoclasts was measured. (F–H) After culturing control and PMCA-silenced BMMs for 2 d with RANKL and M-CSF, cells were transfected with control or nNOS-siRNA oligonucleotides. Cells were further cultured with RANKL and M-CSF for 3 d. (F) After 5 d of culture, osteoclastogenesis was assessed by TRAP staining. Bars, 50 μm. (G) The knockdown of PMCA1, PMCA4, and nNOS was confirmed by Western blotting. (H) The fusion index was calculated from the cells in F. All quantitative data are means ± SD, representative of three experiments performed in triplicate (*, $P < 0.05$; **, $P < 0.01$).

Although both isoforms were expressed in osteoclasts, PMCA1 and PMCA4 do not seem to be functionally redundant. The siRNA-mediated specific knockdown of either isoform of PMCA alone was sufficient to significantly enhance Ca^{2+} oscillations and osteoclast differentiation (Figs. 2 and 3). Furthermore, PMCA4 but not PMCA1 was involved in the regulation of NO, which is suggested to enhance osteoclast fusion. In RANKL-treated osteoclast precursors, only PMCA4 was coimmunoprecipitated with nNOS (Fig. 6 B), which is in accordance with previous studies that showed a physical interaction between PMCA4 and nNOS in smooth muscle cells (Schuh et al., 2003) and the inhibition of nNOS by PMCA4 caused by a local decrease in Ca^{2+} concentration (Schuh et al., 2001). The importance of PMCA–nNOS interaction in osteoclast fusion was clearly demonstrated by the dramatic decrease in the osteoclast fusion induced by PMCA4 knockdown in the absence of

Published December 24, 2012

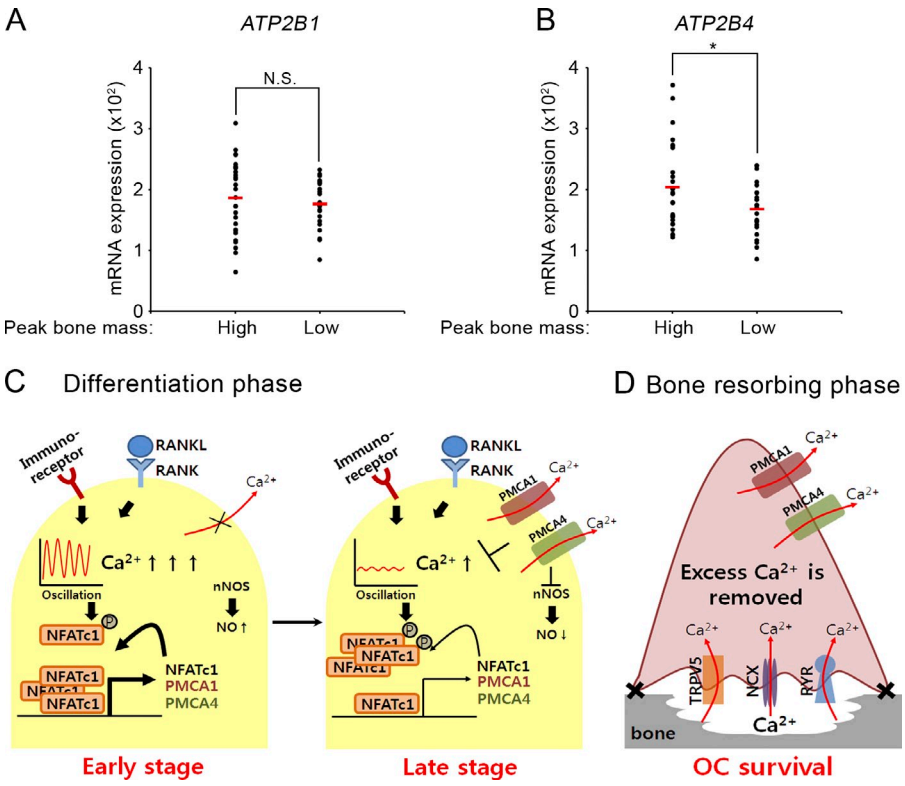

Figure 7. **Elevated *ATP2B4* gene expression correlates with high peak bone mass in humans.** (A and B) *ATP2B1* and *ATP2B4* mRNA expression levels were analyzed from gene expression dataset GSE7158 deposited in GEO. The difference in mRNA expression between high and low peak bone mass groups was analyzed by Mann-Whitney *U* test (*, $P < 0.05$). (C) During the early stage of osteoclast differentiation, increased intracellular Ca^{2+} concentrations trigger NFATc1 autoamplification and PMCA transcription. In the late stage of osteoclast differentiation, increased PMCAs expel cytosolic Ca^{2+}, diminishing Ca^{2+} oscillations and attenuating NFATc1 activation. PMCA4 possesses an additional inhibitory role in osteoclastogenesis by inhibiting NO production in osteoclast precursors. (D) In mature bone-resorbing osteoclasts, increased PMCAs discharge Ca^{2+} across basolateral membrane in favor of osteoclast survival in the face of massive Ca^{2+} entry upon bone resorption.

nNOS (Fig. 6 H). Thus, our data indicate that PMCA4 has a unique role of NO regulation during osteoclastogenesis, in addition to the modulation of Ca^{2+}–NFATc1 axis. Notably, the expression level of PMCA4 rather than that of PMCA1 exhibited a higher correlation with peak bone mass in women (Fig. 7, A and B). The precise underlying mechanisms by which bone mass is regulated by PMCAs in humans, including the possible involvement of NO, need to be investigated in further studies.

To summarize, we propose dual roles of PMCAs during osteoclastogenesis (Fig. 7, C and D). During osteoclast differentiation (Fig. 7 C), NFATc1 increases PMCA expression in a RANKL-dependent manner. In late stages of osteoclast differentiation, high levels of PMCA cause efflux of intracellular Ca^{2+}, reducing Ca^{2+} oscillations and limiting NFATc1 activities. This autoregulatory loop consisting of NFATc1, PMCA, and Ca^{2+} oscillations fine-tunes osteoclastogenesis. An additional mode of osteoclastogenesis regulation exists in which PMCA4 inhibits NO production that expedites osteoclast fusion. Therefore, PMCAs may limit excessive osteoclast formation by lowering intracellular Ca^{2+} and NO. In bone-resorbing osteoclasts (Fig. 7 D), maximal PMCA expression ensures osteoclast survival by the extrusion of excessive Ca^{2+} across the basolateral membrane in the face of massive Ca^{2+} entry upon bone resorption. An osteopenic bone phenotype was observed in both *Atp2b1*$^{+/-}$ and *Atp2b4*$^{-/-}$ mice, suggesting that in the absence of PMCA the advantageous conditions for osteoclast differentiation dominated over adverse effects on osteoclast survival in vivo. Because PMCA4 expression correlated with high peak bone mass in women, the modulation of PMCA4 expression or activity might serve as a novel strategy against bone erosive diseases such as osteoporosis.

Materials and methods

Reagents

Recombinant human soluble RANKL and human M-CSF were purchased from PeproTech. Lipofectamine 2000 and Fura-2/AM were purchased from Invitrogen. Antibodies against PMCAs were purchased from Santa Cruz Biotechnology, Inc. (pan-PMCA) and Thermo Fisher Scientific (PMCA1 and PMCA4). Phospho-specific antobodies for p38, ERK1/2, JNK, CREB, and PLCγ1 were obtained from Cell Signaling Technology. Antibodies against p38, ERK1/2, JNK, c-Jun, PLCγ1, and cleaved caspases-3 were also purchased from Cell Signaling Technology. Antibodies for c-Fos, NFATc1, tubulin, PARP, and lamin B were obtained from Santa Cruz Biotechnology, Inc. Anti–β-actin, FITC-conjugated cholera toxin B subunit, ionomycin, eosin Y, the leukocyte acid phosphatase assay kit, and all other chemicals were obtained from Sigma-Aldrich.

Animals and in vitro osteoclastogenesis

The mutant PMCA1 (*Atp2b1*) and PMCA4 (*Atp2b4*) lines were prepared and maintained on the mixed (129Svj and Blackswiss) genetic background as previously described (Okunade et al., 2004). Loss of both copies of *Atp2b1* caused embryonic lethality, but heterozygous mutants had no observable disease phenotype. *Atp2b4*$^{-/-}$ mutant mice showed no embryonic lethality and appeared externally normal. Although *Atp2b1*$^{+/-}$ mice and wild-type littermates were generated by breeding *Atp2b1*$^{+/-}$ and wild-type breeder-mates, *Atp2b4*$^{-/-}$ and wild-type littermates were generated by crossing *Atp2b4*$^{+/-}$ mice; genotypes were confirmed by PCR analysis using primers previously described (Okunade et al., 2004). All mice were maintained and procedures were performed as per guidelines by the National Institutes of Health (Guide for the Care and Use of Laboratory Animals). Animal experiment protocols were approved by the Committees on the Care and Use of Animals in Research at Seoul National University and University of Cincinnati. BMMs obtained from 5-wk-old ICR or PMCA mutant mice were used as osteoclast precursor cells for in vitro osteoclastogenesis experiments as described previously (Lee et al., 2008). In brief, mouse whole bone marrow cells, isolated by flushing the marrow space of femora and tibiae, were incubated overnight on culture dishes in α–modified Eagle medium (α-MEM) supplemented with 10% FBS. After discarding adherent cells, floating cells were further incubated with M-CSF (30 ng/ml) on Petri dishes. BMMs became adherent after a 3-d culture and were used as osteoclast precursor cells. Upon incubation of BMMs (3×10^4 cells/well in 48-well plates) with 30 ng/ml M-CSF and 100 ng/ml RANKL, >80% of

Published December 24, 2012

the total cells became mononuclear TRAP-positive cells (preosteoclasts) after 2 d of culture. Fully mature multinucleated osteoclasts were formed after further incubation for 1 or 2 d. The osteoclast fusion index was defined as the number of nuclei per one multinucleated osteoclast (Kaneda et al., 2000). The exact time required for full differentiation varied slightly between experiments, and osteoclastogenesis was generally slower in transfected or virus-infected cells. To purify mature osteoclasts, BMMs (10^7 cells) were differentiated into osteoclast on collagen gel-coated 10-cm culture dishes in the presence of 30 ng/ml M-CSF and 100 ng/ml RANKL. Osteoclasts were detached by treating 0.2% collagenase (Invitrogen) at 37°C for 10 min, briefly centrifuged, and replated on culture dishes to allow reattachment for 1 h at 37°C. After the second round of collagenase treatment and gentle pipetting, only firmly attached mature osteoclasts remained whereas osteoclast precursors were removed.

Plasmid construction, transfection, and retroviral gene transfer

BMMs were transfected with pcDNA-rPMCA1 constructs (Bhargava et al., 2002) using Lipofectamin 2000. The entire coding region of mouse PMCA4 was PCR amplified from mouse osteoclast cDNA using the forward primer 5′-GGGCTCGAGCCACCATGACGAATCCACCAGGA-3′ and the reverse primer 5′-GGGGCGGCCGCTCAGACCGGTGTCTCCAG-3′. The amplified PCR product was cloned into a pMX-IG vector using XhoI and NotI sites. Retroviral packaging was performed by transfecting Plat-E cells with plasmids using Lipofectamin 2000. At 48 h after transfection, culture medium containing viral particles was collected and filtered through 0.45-µm syringe filters (Sartorius Stedim Biotech). For retroviral infection, BMMs were incubated in the virus-containing medium with 10 µg/ml polybrene and 30 ng/ml M-CSF for 24 h. The infection efficiency was >80% when measured for GFP fluorescence.

Gene knockdown by siRNA

The siRNA duplexes for PMCA1 (NM_026482_stealth_3610), PMCA4 (NM_213616_stealth_1507), and the negative universal control (medium GC content) were purchased from Invitrogen. Oligonucleotide siRNA duplexes were transfected into BMMs with Lipofectamin 2000 according to the manufacturer's protocol.

Gene-expression profiling

The gene profiling of human PBMC-derived osteoclasts was described previously (Chang et al., 2008a). For osteoclast formation, hPBMCs were cultured in the presence of 30 ng/ml M-CSF and 100 ng/ml RANKL for 3 (preosteoclast) or 7 d (mature osteoclast). Total RNAs were extracted from hPBMCs, reverse transcribed, and transcribed in vitro into biotin-labeled cRNAs. These cRNAs were hybridized with the GeneChip Human Genome U133 Plus 2.0 Array (Affymetrix). The array chips were scanned with a GeneArray scanner (Affymetrix) and were analyzed by Microarray Suite 5.0 (Affymetrix). Publicly available gene expression datasets of human samples were downloaded from GEO (accession no. GSE7158) and the correlation between *ATP2B1/ATP2B4* mRNA expression and peak bone mass was analyzed.

Cell-surface biotinylation and LC/MS/MS experiments

BMMs (4×10^5 cells/well in 6-well plates) were cultured with 30 ng/ml M-CSF alone or 200 ng/ml M-CSF plus RANKL for 36 h. A total of 2×10^7 cells were surface biotinylated using the Pinpoint cell-surface protein isolation kit (Thermo Fisher Scientific) following the manufacturer's instructions. After cell lysis, biotinylated proteins were purified using a streptavidin column and subjected to SDS-PAGE. Protein bands showing differential expression were excised, digested with trypsin, and analyzed by nano-LC/MS/MS (Lee et al., 2008) equipped with an LTQ-FT mass spectrometer (Thermo Fisher Scientific) and an 1100 Series NanoLC pump (Agilent Technologies). Data from the mass spectrometer were analyzed using the Bioworks 3.2 software (Thermo Fisher Scientific). The search results were subsequently evaluated by PeptideProphet and home-built software.

Real-time PCR and RT-PCR analyses

For real-time PCR analysis, 1.5 µg of total RNA was reverse transcribed and PCR amplified with SYBR green master mix (Applied Biosystems) for 40 cycles of 15-s denaturation at 95°C and 1-min amplification at 60°C in ABI Prism 7500 System (Applied Biosystems). Relative mRNA expression levels were presented by normalizing against *Hprt1* mRNA levels. For RT-PCR analysis, total RNAs were isolated with TRIzol reagent (Invitrogen) and 2 µg of RNAs were reverse transcribed with Superscript II (Invitrogen) according to the manufacturer's instructions. The primer sets used in real-time PCR and RT-PCR are listed in Table S1.

ChIP

ChIP assays were performed based on the protocol provided by the manufacturer (EZ ChIP kit; EMD Millipore) and the previously published method with slight modifications (Ha et al., 2010). In brief, BMMs were cultured with 30 ng/ml M-CSF and 100 ng/ml RANKL for 48 h to induce NFATc1 expression before cross-linking using formaldehyde. After sonication, the chromatin was immunoprecipitated with 5 µg each of control IgG antibody (Santa Cruz Biotechnology, Inc.) or NFATc1 antibody (Santa Cruz Biotechnology, Inc.). The eluted DNA fragments were analyzed by PCR using specific primers flanking the NFATc1 binding sites located within ∼1.5 kb upstream of *Atp2b1* or *Atp2b4* transcription initiation sites. Putative NFATc1 binding sites were identified using the web-based prediction program PROMO. Two putative NFATc1 binding sites of *Atp2b1* promoter region (−1,103 to −1,092 and −52 to −44) and four putative NFATc1 binding sites of *Atp2b4* promoter region (−1,292 to −1,283, −1,161 to −1,153, −1,047 to −1,039, and −51 to −43) were identified. PCR primer sequences are listed in Table S2. Input samples were also subjected to PCR with the same primers.

Western blotting and Immunoprecipitation

Western blotting and immunoprecipitation experiments were performed as previously described (Ryu et al., 2006; Kim et al., 2007). Cells were disrupted in lysis buffer (50 mM Tris, pH 7.4, 150 mM NaCl, 1.5 mM $MgCl_2$, 1 mM EGTA, 1% Triton X-100, 10 mM NaF, 1 mM Na_3VO_4, and complete protease inhibitor cocktail) and 30 or 45 µg of cell lysates were resolved by 8–10% SDS-PAGE. Separated proteins were transferred to a polyvinylidene difluoride membrane (GE Healthcare) and the membrane was blocked with 5% skim milk and probed with appropriate primary antibodies. After 1-h incubation with HRP-conjugated secondary antibodies, the immunoreactivity was detected using chemiluminescence. For coimmunoprecipitation experiments, 1 mg of cell lysates was immunoprecipitated with 2 µg of anti-PMCA1 or anti-PMCA4 antibodies and immunoblotted using nNOS or pan-PMCA antibodies. Control immunoprecipitation was performed using a mouse IgG isotype control antibody. Nuclear fractions were prepared by lysing cells in a hypotonic lysis buffer (10 mM Hepes, pH 7.9, 1.5 mM $MgCl_2$, 10 mM KCl, and 0.5 mM PMSF) and solubilizing nuclear pellets with the sequential addition of 15 µl of high salt buffer (20 mM Hepes, pH 7.9, 420 mM NaCl, 25% glycerol, 1.5 mM $MgCl_2$, 0.2 mM EDTA, 0.5 mM PMSF, and 0.5 mM DTT) and 75 µl of storage buffer (20 mM Hepes, pH 7.9, 100 mM NaCl, 20% glycerol, 0.2 mM EDTA, 0.5 mM PMSF, and 0.5 mM DTT). Protein concentration was determined using a detergent-compatible protein assay kit (Bio-Rad Laboratories).

Confocal microscopy

To detect the NFATc1 localization, preosteoclasts cultured on glass coverslips were fixed with 3.7% formaldehyde and permeabilized with 0.1% triton X-100. After blocking in PBS containing 1% BSA, coverslips were incubated with anti-laminB or anti-NFATc1 antibodies diluted (1:50, 1 h) in PBS containing 1% BSA for 2 h. Subsequently, cells were washed and stained with DAPI or Cy3-conjugated secondary antibodies (1:300, 1 h). For the measurement of PMCA localization, osteoclasts cultured on dentin discs were fixed and stained with FITC-conjugated cholera toxin (for GM1-containing plasma membrane labeling, 2.5 µg/ml, 20 min) plus anti–pan-PMCA antibodies. After washing, cells on dentin discs were mounted and images were obtained using a confocal microscope (FV300; Olympus).

Measurement of intracellular Ca^{2+} concentrations

BMMs on glass coverslips were cultured with 30 ng/ml M-CSF and 100 ng/ml RANKL for 48 h. For the measurement of Ca^{2+} oscillations in individual osteoclast precursor, cells were loaded with 5 µM Fura-2/AM and 0.05% pluronic F127 for 40 min at room temperature. After washing three times with Hank's balanced salt solution (Gibco), the fluorescence was recorded at every 500 ms with 340/380 nm excitations and 510 nm emission at 37°C using a digital imaging system (Cascade 650; Photometrics) and Metafluor image analysis software (Universal Imaging).

Calcein-xylenol orange double labeling

To evaluate the mineral apposition rate in vivo, *Atp2b1*$^{+/-}$, *Atp2b4*$^{-/-}$, and wild-type littermate mice were sequentially injected with 25 mg/kg calcein and 90 mg/kg xylenol orange intraperitoneally with an interval of 6 d (Lee et al., 2009). At 3 d after the last injection, mice were killed and dissected tibiae were embedded in methyl methacrylate resins. Tissue sections were observed under a laser-scanning microscope (LSM5 PASCAL; Carl Zeiss).

Published December 24, 2012

Osteoblast differentiation

Calvarial cells were isolated from 1-d-old mice as described previously (Lee et al., 2009). Osteoblast differentiation was induced by culturing cells in osteogenic medium (α-MEM containing 10 mM β-glycerophosphate and 100 µg/ml ascorbic acid) for 7 d, which was confirmed by AP staining.

Cytotoxicity assay

The cytotoxicity of eosin on BMMs was assessed using CCK-8 reagents (Dojindo Laboratories) that produce formazan dye in the presence of live cells. The optical density was measured at 450 nm.

Lipopolysaccharide-induced bone resorption in vivo

Mice were injected with 5 mg/kg LPS (from *Escherichia coli* 0111:B4; Sigma-Aldrich) intraperitoneally twice with a 4-d interval as described previously (Chang et al., 2008b). 30 µl of 5 mM eosin were injected at the proximal ends of tibiae twice with a 4-d interval. At 7 d after the first injection, mice were killed and tibiae sections were stained for TRAP activity.

Calvarial bone resorption assay in vivo

Control or PMCA siRNA oligonucleotides (20 µM, 30 µl) were mixed with 10 µl Lipofectamine 2000 and injected into the subcutaneous space of calvariae of 5-wk-old ICR mice three times with 2-d intervals. As a positive control for bone resorption, collagen matrices soaked with RANKL (10 µg) were implanted on the periosteal surface of calvariae. At 6 d after final siRNA injection, mice were killed and calvariae were subjected to µCT or processed for histological analyses.

Bone histomorphometry

Bone histomorphometric analyses were performed on paraffin-embedded sections as described previously (Chang et al., 2008b). In brief, calvariae or tibiae were fixed in 4% paraformaldehyde, decalcified in 12% EDTA for 4 wk, and embedded in paraffin. 5-µm-thick tissue sections were subjected to TRAP staining or hematoxylin/eosin staining according to standard procedures. For the measurements of mineralized bones, tibiae were fixed in 4% paraformaldehyde, dehydrated in graded ethanol, and embedded in methyl methacrylate resin. Sections of 5 µm thickness were subjected to von Kossa's silver nitrate staining followed by van Gieson's counterstaining.

µCT analysis

Femurs of 6-wk-old male *Atp2b1*$^{+/-}$, *Atp2b4*$^{-/-}$, and wild-type littermate mice were analyzed by µCT using the SkyScan 1072 system (SkyScan). Trabecular bone volume was measured in the 1-mm region in length, 1 mm below the distal growth plate of femurs. A total of 350–400 tomographic slices were acquired and 3D analyses were performed with CT volume software (ver 1.11; SkyScan).

Detection of apoptosis in vivo and in vitro by TUNEL assay

TUNEL assay using In situ Cell Death Detection kit (Roche) coupled to an AP-conjugated antobody was performed on bone tissue sections of 6-wk-old male *Atp2b1*$^{+/-}$, *Atp2b4*$^{-/-}$, and wild-type littermate mice to evaluate in vivo osteoclast apoptosis. For the detection of in vitro osteoclast apoptosis, mature osteoclasts were purified from the co-cultures of mouse bone marrow cells and calvarial osteoblasts (Ha et al., 2004). After transferring onto dentine discs (Immunodiagnostic Systems), mature osteoclasts (2×10^2 cells/disc) were transfected with PMCA siRNA oligonucleotides and further cultured with 30 ng/ml M-CSF and 100 ng/ml RANKL for 2 d. TUNEL assay with In situ Cell Death Detection kit coupled to an FITC-conjugated antibody was performed followed by Cy3-conjugated phalloidin (Invitrogen) and DAPI (Invitrogen) staining.

NO measurements

BMMs on glass coverslips were transfected with control or isoform-specific PMCA siRNAs and were further cultured with 30 ng/ml M-CSF and 100 ng/ml RANKL for 2 d. Cells were loaded with 5 µM of the cell-permeable fluorescent NO indicator DAF-2 DA (EMD Millipore) for 30 min. NO-dependent fluorescence was observed under a laser-scanning microscope. To confirm the specificity of DAF-2 DA fluorescence, cells were cultured overnight with 100 ng/ml LPS in the absence or presence of a NO synthase inhibitor, L-NMMA (10 µM; EMD Millipore), for 2 h before DAF-2 DA loading.

Statistical analysis

The Student's *t* test was used to determine the significance of differences between two groups. Comparison of multiple results was performed by one-way analysis of variance followed by Student Knewman-Keuls post hoc tests. Differences with $P < 0.05$ were regarded as significant. The gene expression data in Fig. 7 were analyzed by Mann-Whitney *U* test.

Online supplemental material

Fig. S1 shows the effect of PMCA knockdown on osteoclastogenesis in calvariae organ culture models. Fig. S2 shows the enhanced RANKL-induced Ca^{2+} oscillations and osteoclast differentiation upon eosin treatment in vitro and in vivo. Fig. S3 shows the changes in P38, ERK1/2, JNK1/2, and PLCγ1 phosphorylation as well as c-Fos expression after RANKL stimulation in PMCA knocked down cells by Western blotting. Fig. S4 shows no change in osteoblast differentiation after PMCA knockdown or inhibition in vitro. Fig. S5 shows the expression levels of SERCA2 and TRPV5 in PMCA knocked down cells by Western blotting. Table S1 lists primer sets used in real-time PCR and RT-PCR experiments. Table S2 shows PCR primer sequences used in ChIP experiments. Online supplemental material is available at http://www.jcb.org/cgi/content/full/jcb.201204067/DC1.http://www.jcb.org/cgi/content/full/jcb.201204067/DC1

This work was supported by grants from the Science Research Center (20120000490) and the Ministry of Health and Welfare (A111787) to H.-H. Kim, and the Korea Research Foundation grants funded by the Korean government (KRF-2008-313-E00439 and NRF-2010-359-E00016 to Y. Lee and NRF-2010-860-20100096 to H.J. Kim). V. Prasad was supported by American Heart Association 11BGIA7720005 and National Institutes of Health grant HL061974.

The authors declare no conflict of interest.

Submitted: 13 April 2012
Accepted: 21 November 2012

References

Asagiri, M., K. Sato, T. Usami, S. Ochi, H. Nishina, H. Yoshida, I. Morita, E.F. Wagner, T.W. Mak, E. Serfling, and H. Takayanagi. 2005. Autoamplification of NFATc1 expression determines its essential role in bone homeostasis. *J. Exp. Med.* 202:1261–1269. http://dx.doi.org/10.1084/jem.20051150

Bekker, P.J., and C.V. Gay. 1990. Biochemical characterization of an electrogenic vacuolar proton pump in purified chicken osteoclast plasma membrane vesicles. *J. Bone Miner. Res.* 5:569–579. http://dx.doi.org/10.1002/jbmr.5650050606

Berger, C.E., H. Rathod, J.I. Gillespie, B.R. Horrocks, and H.K. Datta. 2001. Scanning electrochemical microscopy at the surface of bone-resorbing osteoclasts: evidence for steady-state disposal and intracellular functional compartmentalization of calcium. *J. Bone Miner. Res.* 16:2092–2102. http://dx.doi.org/10.1359/jbmr.2001.16.11.2092

Bhargava, A., R.S. Mathias, J.A. McCormick, M.F. Dallman, and D. Pearce. 2002. Glucocorticoids prolong $Ca^{(2+)}$ transients in hippocampal-derived H19-7 neurons by repressing the plasma membrane $Ca^{(2+)}$-ATPase-1. *Mol. Endocrinol.* 16:1629–1637. http://dx.doi.org/10.1210/me.16.7.1629

Boyle, W.J., W.S. Simonet, and D.L. Lacey. 2003. Osteoclast differentiation and activation. *Nature*. 423:337–342. http://dx.doi.org/10.1038/nature01658

Brini, M. 2009. Plasma membrane $Ca^{(2+)}$-ATPase: from a housekeeping function to a versatile signaling role. *Pflugers Arch.* 457:657–664. http://dx.doi.org/10.1007/s00424-008-0505-6

Buch, M.H., A. Pickard, A. Rodriguez, S. Gillies, A.H. Maass, M. Emerson, E.J. Cartwright, J.C. Williams, D. Oceandy, J.M. Redondo, et al. 2005. The sarcolemmal calcium pump inhibits the calcineurin/nuclear factor of activated T-cell pathway via interaction with the calcineurin A catalytic subunit. *J. Biol. Chem.* 280:29479–29487. http://dx.doi.org/10.1074/jbc.M501326200

Cartwright, E.J., D. Oceandy, and L. Neyses. 2009. Physiological implications of the interaction between the plasma membrane calcium pump and nNOS. *Pflugers Arch.* 457:665–671. http://dx.doi.org/10.1007/s00424-008-0455-z

Chami, M., D. Ferrari, P. Nicotera, P. Paterlini-Bréchot, and R. Rizzuto. 2003. Caspase-dependent alterations of Ca^{2+} signaling in the induction of apoptosis by hepatitis B virus X protein. *J. Biol. Chem.* 278:31745–31755. http://dx.doi.org/10.1074/jbc.M304202200

Chang, E.J., J. Ha, H. Huang, H.J. Kim, J.H. Woo, Y. Lee, Z.H. Lee, J.H. Kim, and H.H. Kim. 2008a. The JNK-dependent CaMK pathway restrains the reversion of committed cells during osteoclast differentiation. *J. Cell Sci.* 121:2555–2564. http://dx.doi.org/10.1242/jcs.028217

Chang, E.J., J. Ha, F. Oerlemans, Y.J. Lee, S.W. Lee, J. Ryu, H.J. Kim, Y. Lee, H.M. Kim, J.Y. Choi, et al. 2008b. Brain-type creatine kinase has a crucial role in osteoclast-mediated bone resorption. *Nat. Med.* 14:966–972. http://dx.doi.org/10.1038/nm.1860

Clapham, D.E. 2007. Calcium signaling. *Cell*. 131:1047–1058. http://dx.doi.org/10.1016/j.cell.2007.11.028

Published December 24, 2012

Di Leva, F., T. Domi, L. Fedrizzi, D. Lim, and E. Carafoli. 2008. The plasma membrane Ca^{2+} ATPase of animal cells: structure, function and regulation. *Arch. Biochem. Biophys.* 476:65–74. http://dx.doi.org/10.1016/j.abb.2008.02.026

Gatto, C., and M.A. Milanick. 1993. Inhibition of the red blood cell calcium pump by eosin and other fluorescein analogues. *Am. J. Physiol.* 264:C1577–C1586.

Gatto, C., C.C. Hale, W. Xu, and M.A. Milanick. 1995. Eosin, a potent inhibitor of the plasma membrane Ca pump, does not inhibit the cardiac Na-Ca exchanger. *Biochemistry*. 34:965–972. http://dx.doi.org/10.1021/bi00003a031

Ha, H., H.B. Kwak, S.W. Lee, H.M. Jin, H.M. Kim, H.H. Kim, and Z.H. Lee. 2004. Reactive oxygen species mediate RANK signaling in osteoclasts. *Exp. Cell Res.* 301:119–127. http://dx.doi.org/10.1016/j.yexcr.2004.07.035

Ha, J., H.S. Choi, Y. Lee, H.J. Kwon, Y.W. Song, and H.H. Kim. 2010. CXC chemokine ligand 2 induced by receptor activator of NF-kappa B ligand enhances osteoclastogenesis. *J. Immunol.* 184:4717–4724. http://dx.doi.org/10.4049/jimmunol.0902444

Kaneda, T., T. Nojima, M. Nakagawa, A. Ogasawara, H. Kaneko, T. Sato, H. Mano, M. Kumegawa, and Y. Hakeda. 2000. Endogenous production of TGF-beta is essential for osteoclastogenesis induced by a combination of receptor activator of NF-kappa B ligand and macrophage-colony-stimulating factor. *J. Immunol.* 165:4254–4263.

Kim, H.J., Y. Lee, E.J. Chang, H.M. Kim, S.P. Hong, Z.H. Lee, J. Ryu, and H.H. Kim. 2007. Suppression of osteoclastogenesis by N,N-dimethyl-D-erythro-sphingosine: a sphingosine kinase inhibition-independent action. *Mol. Pharmacol.* 72:418–428. http://dx.doi.org/10.1124/mol.107.034173

Kim, K., J.H. Kim, J. Lee, H.M. Jin, S.H. Lee, D.E. Fisher, H. Kook, K.K. Kim, Y. Choi, and N. Kim. 2005. Nuclear factor of activated T cells c1 induces osteoclast-associated receptor gene expression during tumor necrosis factor-related activation-induced cytokine-mediated osteoclastogenesis. *J. Biol. Chem.* 280:35209–35216. http://dx.doi.org/10.1074/jbc.M505815200

Kuroda, Y., C. Hisatsune, T. Nakamura, K. Matsuo, and K. Mikoshiba. 2008. Osteoblasts induce Ca^{2+} oscillation-independent NFATc1 activation during osteoclastogenesis. *Proc. Natl. Acad. Sci. USA*. 105:8643–8648. http://dx.doi.org/10.1073/pnas.0800642105

Lee, Y., S.W. Hyung, H.J. Jung, H.J. Kim, J. Staerk, S.N. Constantinescu, E.J. Chang, Z.H. Lee, S.W. Lee, and H.H. Kim. 2008. The ubiquitin-mediated degradation of Jak1 modulates osteoclastogenesis by limiting interferon-beta-induced inhibitory signaling. *Blood*. 111:885–893. http://dx.doi.org/10.1182/blood-2007-03-082941

Lee, Y., J. Ha, H.J. Kim, Y.S. Kim, E.J. Chang, W.J. Song, and H.H. Kim. 2009. Negative feedback Inhibition of NFATc1 by DYRK1A regulates bone homeostasis. *J. Biol. Chem.* 284:33343–33351. http://dx.doi.org/10.1074/jbc.M109.042234

Lee, Y., H.J. Kim, C.K. Park, W.S. Kim, Z.H. Lee, and H.H. Kim. 2012. Novel extraneural role of neurite outgrowth inhibitor A: modulation of osteoclastogenesis via positive feedback regulation of nuclear factor of activated T cell cytoplasmic 1. *J. Bone Miner. Res.* 27:1043–1054. http://dx.doi.org/10.1002/jbmr.1561

Li, J.P., H. Kajiya, F. Okamoto, A. Nakao, T. Iwamoto, and K. Okabe. 2007. Three Na+/Ca^{2+} exchanger (NCX) variants are expressed in mouse osteoclasts and mediate calcium transport during bone resorption. *Endocrinology*. 148:2116–2125. http://dx.doi.org/10.1210/en.2006-1321

Lorget, F., S. Kamel, R. Mentaverri, A. Wattel, M. Naassila, M. Maamer, and M. Brazier. 2000. High extracellular calcium concentrations directly stimulate osteoclast apoptosis. *Biochem. Biophys. Res. Commun.* 268:899–903. http://dx.doi.org/10.1006/bbrc.2000.2229

Moonga, B.S., R. Davidson, L. Sun, O.A. Adebanjo, J. Moser, M. Abedin, N. Zaidi, C.L. Huang, and M. Zaidi. 2001. Identification and characterization of a sodium/calcium exchanger, NCX-1, in osteoclasts and its role in bone resorption. *Biochem. Biophys. Res. Commun.* 283:770–775. http://dx.doi.org/10.1006/bbrc.2001.4870

Moonga, B.S., S. Li, J. Iqbal, R. Davidson, V.S. Shankar, P.J. Bevis, A. Inzerillo, E. Abe, C.L. Huang, and M. Zaidi. 2002. Ca($^{2+}$) influx through the osteoclastic plasma membrane ryanodine receptor. *Am. J. Physiol. Renal Physiol.* 282:F921–F932.

Nilforoushan, D., A. Gramoun, M. Glogauer, and M.F. Manolson. 2009. Nitric oxide enhances osteoclastogenesis possibly by mediating cell fusion. *Nitric Oxide*. 21:27–36. http://dx.doi.org/10.1016/j.niox.2009.04.002

Nowycky, M.C., and A.P. Thomas. 2002. Intracellular calcium signaling. *J. Cell Sci.* 115:3715–3716. http://dx.doi.org/10.1242/jcs.00078

Okunade, G.W., M.L. Miller, G.J. Pyne, R.L. Sutliff, K.T. O'Connor, J.C. Neumann, A. Andringa, D.A. Miller, V. Prasad, T. Doetschman, et al. 2004. Targeted ablation of plasma membrane Ca^{2+}-ATPase (PMCA) 1 and 4 indicates a major housekeeping function for PMCA1 and a critical role in hyperactivated sperm motility and male fertility for PMCA4. *J. Biol. Chem.* 279:33742–33750. http://dx.doi.org/10.1074/jbc.M404628200

Pellegrini, L., and L. Scorrano. 2007. A cut short to death: Parl and Opa1 in the regulation of mitochondrial morphology and apoptosis. *Cell Death Differ.* 14:1275–1284. http://dx.doi.org/10.1038/sj.cdd.4402145

Ryu, J., H.J. Kim, E.J. Chang, H. Huang, Y. Banno, and H.H. Kim. 2006. Sphingosine 1-phosphate as a regulator of osteoclast differentiation and osteoclast-osteoblast coupling. *EMBO J.* 25:5840–5851. http://dx.doi.org/10.1038/sj.emboj.7601430

Salo, J., P. Lehenkari, M. Mulari, K. Metsikkö, and H.K. Väänänen. 1997. Removal of osteoclast bone resorption products by transcytosis. *Science*. 276:270–273. http://dx.doi.org/10.1126/science.276.5310.270

Schuh, K., S. Uldrijan, M. Telkamp, N. Rothlein, and L. Neyses. 2001. The plasmamembrane calmodulin-dependent calcium pump: a major regulator of nitric oxide synthase I. *J. Cell Biol.* 155:201–205. http://dx.doi.org/10.1083/jcb.200104131

Schuh, K., T. Quaschning, S. Knauer, K. Hu, S. Kocak, N. Roethlein, and L. Neyses. 2003. Regulation of vascular tone in animals overexpressing the sarcolemmal calcium pump. *J. Biol. Chem.* 278:41246–41252. http://dx.doi.org/10.1074/jbc.M307606200

Schuh, K., E.J. Cartwright, E. Jankevics, K. Bundschu, J. Liebermann, J.C. Williams, A.L. Armesilla, M. Emerson, D. Oceandy, K.P. Knobeloch, and L. Neyses. 2004. Plasma membrane Ca^{2+} ATPase 4 is required for sperm motility and male fertility. *J. Biol. Chem.* 279:28220–28226. http://dx.doi.org/10.1074/jbc.M312599200

Sharma, S.M., A. Bronisz, R. Hu, K. Patel, K.C. Mansky, S. Sif, and M.C. Ostrowski. 2007. MITF and PU.1 recruit p38 MAPK and NFATc1 to target genes during osteoclast differentiation. *J. Biol. Chem.* 282:15921–15929. http://dx.doi.org/10.1074/jbc.M609723200

Shinohara, M., T. Koga, K. Okamoto, S. Sakaguchi, K. Arai, H. Yasuda, T. Takai, T. Kodama, T. Morio, R.S. Geha, et al. 2008. Tyrosine kinases Btk and Tec regulate osteoclast differentiation by linking RANK and ITAM signals. *Cell*. 132:794–806. http://dx.doi.org/10.1016/j.cell.2007.12.037

Takayanagi, H., S. Kim, T. Koga, H. Nishina, M. Isshiki, H. Yoshida, A. Saiura, M. Isobe, T. Yokochi, J. Inoue, et al. 2002. Induction and activation of the transcription factor NFATc1 (NFAT2) integrate RANKL signaling in terminal differentiation of osteoclasts. *Dev. Cell*. 3:889–901. http://dx.doi.org/10.1016/S1534-5807(02)00369-6

van der Eerden, B.C., J.G. Hoenderop, T.J. de Vries, T. Schoenmaker, C.J. Buurman, A.G. Uitterlinden, H.A. Pols, R.J. Bindels, and J.P. van Leeuwen. 2005. The epithelial Ca^{2+} channel TRPV5 is essential for proper osteoclastic bone resorption. *Proc. Natl. Acad. Sci. USA*. 102:17507–17512. http://dx.doi.org/10.1073/pnas.0505789102

Walsh, M.C., N. Kim, Y. Kadono, J. Rho, S.Y. Lee, J. Lorenzo, and Y. Choi. 2006. Osteoimmunology: interplay between the immune system and bone metabolism. *Annu. Rev. Immunol.* 24:33–63. http://dx.doi.org/10.1146/annurev.immunol.24.021605.090646

Yang, S., and Y.P. Li. 2007. RGS10-null mutation impairs osteoclast differentiation resulting from the loss of [Ca^{2+}]i oscillation regulation. *Genes Dev.* 21:1803–1816. http://dx.doi.org/10.1101/gad.1544107

Yang, Y.M., M.S. Kim, A. Son, J.H. Hong, K.H. Kim, J.T. Seo, S.I. Lee, and D.M. Shin. 2009. Alteration of RANKL-induced osteoclastogenesis in primary cultured osteoclasts from $SERCA2^{+/-}$ mice. *J. Bone Miner. Res.* 24:1763–1769. http://dx.doi.org/10.1359/jbmr.090420

Yoon, S.H., Y. Lee, H.J. Kim, Z.H. Lee, S.W. Hyung, S.W. Lee, and H.H. Kim. 2009. Lyn inhibits osteoclast differentiation by interfering with PLCgamma1-mediated Ca^{2+} signaling. *FEBS Lett.* 583:1164–1170. http://dx.doi.org/10.1016/j.febslet.2009.03.005